1995ApJ...444..200S

THE ASTROPHYSICAL JOURNAL, 444:200–206, 1995 May 1

ON THE SUPERSONIC TURBULENCE OF NGC 604

NANCI S. P. SABALISCK, GUILLERMO TENORIO-TAGLE, HÉCTOR O. CASTAÑEDA, AND CASIANA MUÑOZ-TUÑÓN
Instituto de Astrofísica de Canarias, E-38200, La Laguna, Tenerife, Canary Islands, Spain
Received 1994 March 28; accepted 1994 October 24

ABSTRACT

Two-dimensional high spatial resolution Fabry-Perot observations with TAURUS 2 at the William Herschel Telescope in La Palma, over the inner central regions of NGC 604 in M33, have been obtained. The data show a large variety of line profile shapes produced over the region. Some display clear splitting, or strong asymmetries, most likely caused by the action of strong winds and champagne flows produced by the many massive stars presently disrupting large sections of the parent cloud. On the other hand, emission lines arising from the multicore or highest intensity regions of NGC 604 show well-defined Gaussian profiles with a typical FWHM of 38.8 km s^{-1} in Hα, implying an intrinsic supersonic velocity dispersion of 16.5 km s^{-1}. This agrees, within the observational errors, with the global integrated line profile of NGC 604. Here we show that the contribution to the overall line profile from other zones of NGC 604 are negligible. They present a much lower intensity and thus, even if some are fitted with broader Gaussians, they do not contribute appreciably when compared to the higher intensity lines arising from the multicore region.

Subject headings: galaxies: individual (M33) — H II regions — ISM: individual (NGC 604) — ISM: kinematics and dynamics — turbulence

1. INTRODUCTION

NGC 604 is the largest H II region in M33, located at a distance of 720 kpc, and one order of magnitude more massive and luminous than the biggest H II regions in our Galaxy (Drissen 1991). It is located 1.2 kpc southeast from the center of M33, at the edge of a big molecular cloud with an upper limit mass estimate of 3–4 × 10^5 $M_\odot$ (Blitz 1985). Morphologically, the central zone of NGC 604 shows several emitting knots, and a large inhomogeneous halo, where several shells, filaments, and loops (first classified by D'Odorico & Rosa 1981) are distributed. The H I mass in the region is 1.6 × 10^6 $M_\odot$ (Wright 1971), whereas the ionized mass is ∼10^6 $M_\odot$ (Israel et al. 1982), and its integrated Hα luminosity is ≈4.5 × 10^{39} ergs s^{-1} (Melnick 1992).

Embedded in the region are a number of young and massive stars and OB associations, as well as nitrogen and carbon Wolf-Rayet (W-R) stars (see, for example, D'Odorico & Rosa 1981; Drissen, Moffat, & Shara 1990; Debray 1991). Due to the W-R features and the apparent lack of supernovae and SNRs (only one bonafide remnant has been detected by Benvenuti, D'Odorico, & Dumontel 1979), NGC 604 is known to be a very young star-forming region, of ∼4 × 10^6 yr old (D'Odorico & Rosa 1981).

Smith & Weedman (1970) discovered the supersonic velocity dispersion (σ) in the integrated emission line of NGC 604. Later, using Fabry-Perot observations and the integrated profile of the Hβ emission line, Melnick (1980) reported variations in the obtained velocity dispersion at different positions in the nebula, including core and halo areas. From a study of several giant extragalactic H II regions (GEHR) including NGC 604, Terlevich & Melnick (1981) proposed self-gravity as the explanation to the kinematics of these regions. Their main argument was that the size and luminosity of GEHR obey the same correlations with velocity dispersion as found for massive, gravitationally bound systems such as globular clusters and the central regions of elliptical galaxies. Recently, these correlations have been offered an explanation as a direct consequence of massive cluster formation in the cometary stirring model by Tenorio-Tagle, Muñoz-Tuñón, & Cox (1993).

Detailed studies of the effects of stellar winds in the interstellar matter of NGC 604 have been done by Rosa & Solf (1984), Hippelein & Fried (1984), and Clayton (1988). They found several shells, loops, and filaments most likely associated to W-R stars. All of them interpreted their observations within the frame of work put forward by Dyson (1979), i.e., a coeval large burst of massive stars, all of them undergoing strong winds as to compose a giant shell of swept-up matter. More recently, Chu & Kennicutt (1995), among others, have claimed a superposition of hundreds of expanding wind-driven shells as the explanation to the observed supersonic σ.

Other authors, considering the position of the H II regions in relation to their associated molecular clouds, the high-velocity dispersion values found in some parts of the nebula (>25 km s^{-1}), and the complex emission-line profiles observed, have proposed the champagne model as a explanation to the overall observed dynamics (Rosa & Solf 1984; Skillman & Balick 1984; Hunter & Gallagher 1985).

Here we present the analysis of two-dimensional spectra obtained in the lines of Hα and in [O III] λ5007, covering the central 230 pc of NGC 604, while the total diameter of the region is ≈400 pc (Melnick 1992). Our aim is to disentangle the velocity field by separating the main contributors to the dynamics of the system. In this way one could sort out what causes supersonic turbulence in giant H II regions and thus get to know the true nature of regions of violent star formation. Sections 2 and 3 present the data and the data analysis; § 4 provides the main results, and § 5 lists our conclusions.

2. DATA AQUISITION AND REDUCTION

Two-dimensional imaging spectroscopy in Hα and [O III] λ5007 lines was obtained for NGC 604 by means of the TAURUS 2 Fabry-Perot imaging spectrograph (Atherton & Taylor 1980) at the F/4 Cassegrain Focus of the William Herschel Telescope (WHT) of the Observatorio del Roque de los

TABLE 1

MAIN PARAMETERS OF THE OBSERVATIONAL SETUP

Parameter	Hα	[O III]
Wavelength observed (Å)	6562.81	5006.8
Calibration line (Å)	6598.96	5037.75
Free spectral range (km s^{-1})	807	596
$\Delta\lambda$ $step^{-1}$ (km s^{-1})	9.11	7.70
FWHM of the calibration line (km s^{-1})	40	33
Spatial scale (arcsec $pixel^{-1}$)	0.26	0.26

Muchachos, during the nights of 1990 July 31 and 1991 January 31, with the IPCS-II as detector, and the 125 μm etalon, using the same instrumental setup for both observing nights. The IPCS is an ideal detector for this type of work, as the possibility of a fast scanning minimizes the variations in the atmospheric conditions during the observations. The system accumulates each of the frames scanned with this fast scanning mode. The total (cumulative) integration time per frame is 36 s. Typical seeing values during the observing runs was 1″. The Balmer line was selected because it is intrinsically bright, while the oxygen line, having a narrower thermal width, is better suited for velocity dispersion studies.

The format of the data cube was of 256 * 256 * 100, the spatial scale is 0.″26 $pixel^{-1}$. Each integration was of 3600 s (36 s per frame). Four filters were used, two for the lines of observation and two more for the corresponding calibration. Interference filters of zero redshift were used to isolate an order of interference of the Fabry-Perot, the width of the filter being of the same order as the free spectral range (FSR) etalon. The main parameters of the observational setup are summarized in Table 1. The measured instrumental resolution, defined by the finesse (the ratio between the free spectral range and the instrumental line width) was almost the same for both nights (20 for Hα and 18 for [O III] λ5007). A calibration cube for each wavelength was obtained at the beginning of each night and a calibration ring was obtained before and after each observation. These were then compared with the calibration cube, and the correction of the phase map by the effect of mechanical distortions could then be calculated. The result of the phase correction of a raw data cube is a three-dimensional data set where the *x*-*y* axis are the spatial coordinates and the *z*-axis is the calibrated wavelength (the dispersion dimension).

The reduction and analysis of the data was done using TAUCAL (for calibration) and TAUFITS (for automatic fitting), a software package developed by the Royal Greenwich Observatory (Lewis & Unger 1992).

To check our calibration (the zero point of the velocity scale and the line width of the emission lines) we used long-slit high-resolution spectroscopy obtained by the GEFE[1] collaboration with ISIS at the 4.2 m WHT in La Palma. On the brightest positions of the nebula, spectra were extracted to measure the attained line width and central wavelength for Hα and [O III]. Several spectra along the slit position, matching the slit width, were taken and compared with a synthetic TAURUS spectra at the same position. The true FWHM (after instrumental and thermal corrections) was then calculated. We found a systematic and constant difference between the true line widths achieved with the two instruments, of the order of 34.5 km s^{-1} for Hα and 35.2 km s^{-1} for [O III]. The resultant most likely explanation is that the instrumental line width at TAURUS was larger than that estimated at the beginning of the night. After subtracting quadratically these values to the computed σ for the respective wavelengths (after all the corrections for line broadening are taken into account), the final result was adopted as the true velocity dispersion.

3. DATA ANALYSIS

The collapsed image resulting from the compression of the data cube in the spectral direction for each line was used as a base for the preliminary analysis of the data. Using an automatic fitting procedure, three maps in line velocity, line width, and line peak intensity were created. The procedure followed is to fit Gaussians to the spectrum associated to each point, within square areas defined by boxes of 7 × 7 pixels size (equivalent to 1.″8 × 1.″8). The line width map was used as a new base to limit the fitting to those areas where the line width was equal or larger than the instrumental line width.

Looking in detail the line shapes all over the emitting area, there are zones which display asymmetric lines and even splitted profiles. In particular, those coincident with looplike patterns show typical line splitting as expected from bubble-like structures.

We know those positions on the emitting area with well-behaved (single Gaussian) line profiles and their corresponding line flux. The fitting of one single Gaussian to splitted profiles provides a "theoretical" value for the line peak (close to the line centroid) and a meaningless estimation for the line width. Nevertheless, the integrated area of the fitted line can be used as a reasonably good value for the line flux, allowing to estimate its relative importance compared with the integrated spectra of the nebula.

4. DISCUSSION

The intensity maps in both emission lines (see Figs. 1*a*–1*b* [Pl. 12]) clearly show the multicore structure (Kennicutt 1984) of NGC 604. Seven well-resolved bright structures (hereafter referred to as knots 1–7, marked as a function of their intensity in Fig. 1*a*) dominate the emission from the central sector of the nebula.

Between the two brightest knots (1 and 2) and elongated in the N-S direction, one finds a low-intensity channel, or jetlike feature. This feature connects the enclosed low-intensity region fanning out toward the south (cavity B) with a similar region toward the north (cavity A) where the highest velocity dispersion values are found. These arise from single Gaussian fits to strongly asymmetric, or even splitted lines, typical of this area. The channel feature extends some 8″ in the N-S direction and shows clear evidence for an asymmetric funneling of matter finding its way through the path of least resistance among the densest parts of the nebula.

The radial velocity maps (not shown here) display a complex structure, with velocity ranges of ∼45 km s^{-1} in Hα and 60 km s^{-1} in [O III]. As discussed in the previous section, in the areas of line splitting the Gaussian fit defines the centroid of the line profile. As we are interested in the analysis of the global velocity field, we adopted those values as the representative radial velocity for the position. Peaks 2, 3, and 5 (see Fig. 1*a*) show a radial velocity gradient of the order of 2 km s^{-1} pc^{-1}, increasing toward central part of the image. The cavities, A and B, and the channel present the highest values of radial velocity, of the

---

[1] GEFE Grupo de Estudios de Formacion Estelar is an international collaboration of astronomers from Spain, the UK, France, Germany, Denmark, and Italy, formed to take advantage of the "International time" granted by Comitè Cientifico Internacional at Observatories in the Canary Islands.

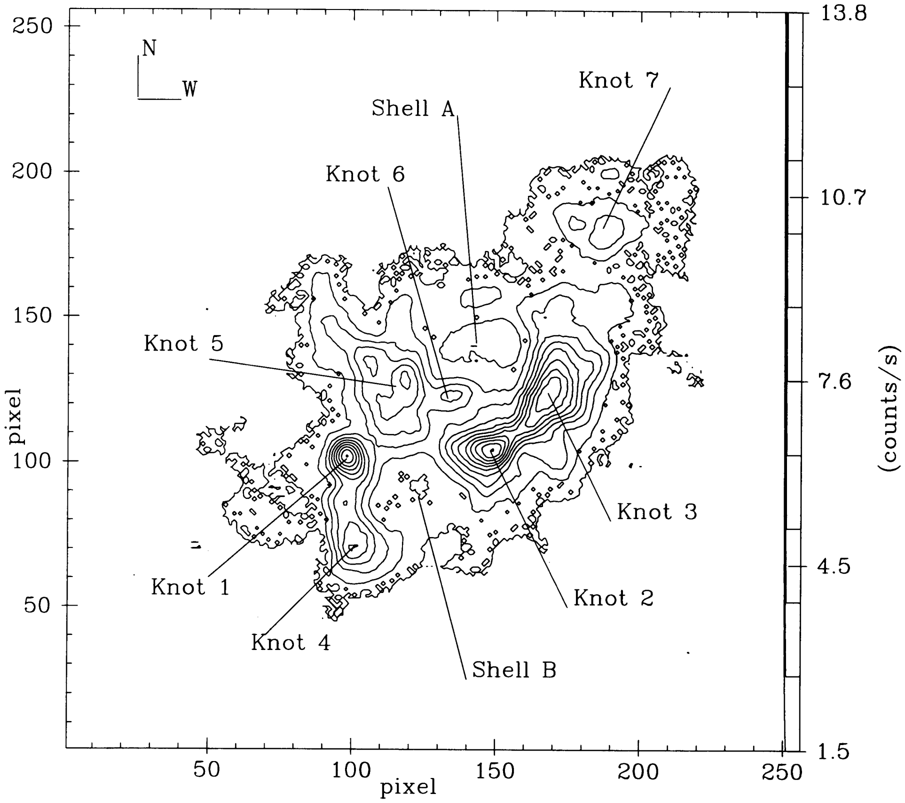

FIG. 1*a*

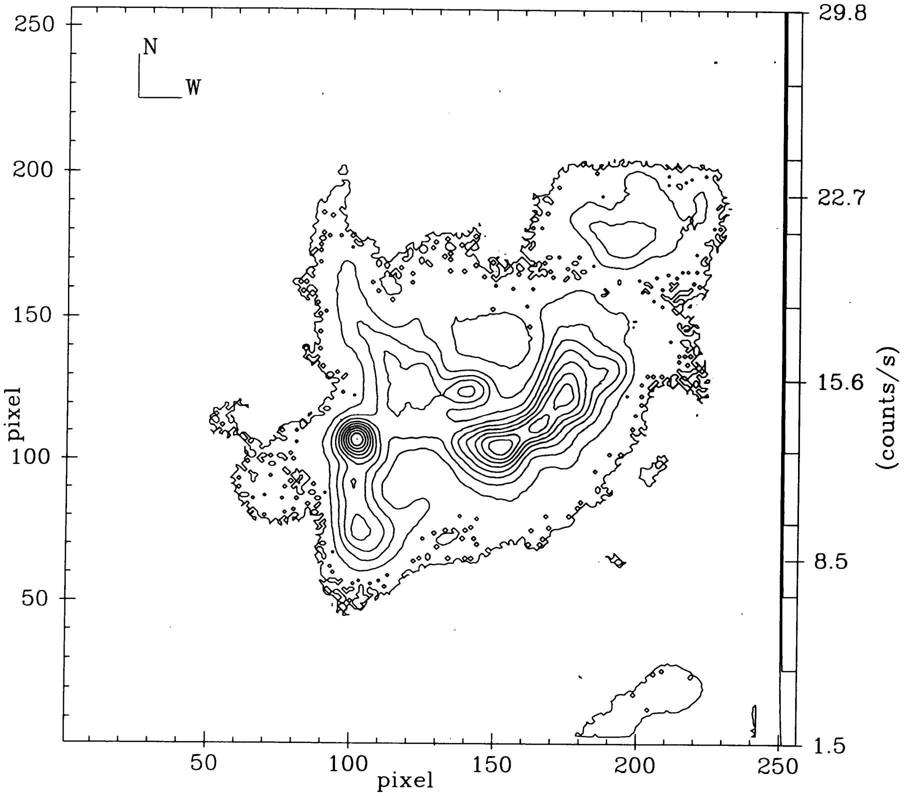

FIG. 1*b*

FIG. 1.—Intensity peak maps of NGC 604. These maps represent the maximum intensity of the Gaussian fit above the background for (*a*) $H\alpha$ and (*b*) [O III] λ5007. In (*a*) are identified the main structures found in NGC 604. Velocity dispersion maps are shown in (*c*) and (*d*) for both emission lines, respectively. These maps are corrected for instrumental and thermal broadening, assuming $T_e = 10{,}000$ K. On the *x*-*y* axes 1 pixel = 0″.26 = 0.91 pc. All maps are created by the program TAUFITS.

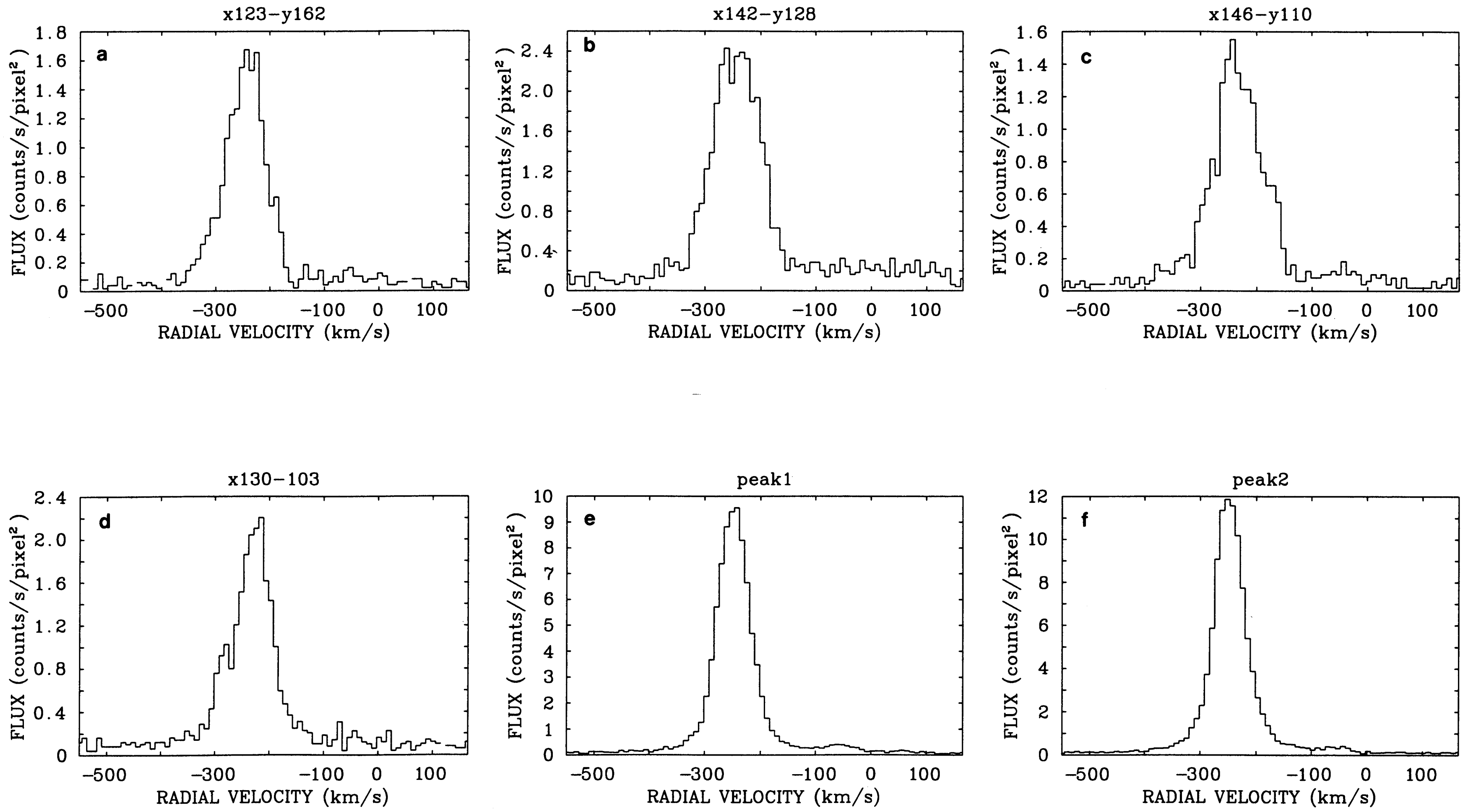

FIG. 2.—Typical spectra obtained for selected positions on (*a*) cavity A, (*b*) central part, (*c*) cavity B, (*d*) a point of the large N-S elongated structure between knots 1 and 2, (*e*) knot 1, (*f*) knot 2

1995ApJ...444..200S

order of ≈ -230 km s^{-1}, while the integrated spectrum of the whole observed area, referred to the heliocentric system of reference, shows a radial velocity of -244 km s^{-1} in Hα and of -240 km s^{-1} in [O III].

The velocity dispersion (σ) maps (Figs. 1*c*–1*d* [Pl. 13]), corrected for instrumental and thermal broadening, assuming $T_e = 10^4$ K, show a large range of σ values, from ≈ 0 to ≈ 50 km s^{-1} in both emission lines. A global velocity dispersion of 17.8 km s^{-1} in the Hα data, and 16.7 km s^{-1} in [O III] is consistent with previously published values (Melnick 1980; Rosa & Solf 1984; Hippelein & Fried 1984).

The highest velocity dispersion values are found in cavity A. A detailed analysis of the spectra of cavity A, cavity B, and channel reveals a large fraction of asymmetric or even multiple line profiles with at least two well-defined emission components. The two main emission components are separated by $\sim$20–40 km s^{-1}. The high-velocity dispersion values obtained for these regions result then from the fitting of single Gaussians to split or strongly asymmetric emission line. Several examples of these are shown in Figures 2*a*–2*d*, and should be compared with Figures 2*e* and 2*f*, profiles obtained from the highest intensity regions (knots 1 and 2, respectively), well fitted with a single Gaussian.

4.1. *Variation of σ with "Aperture"*

The velocity dispersion in NGC 604 is strongly dependent on position within the nebula. Because of this, using different beam sizes simulating concentric apertures (ranging from 2″ to 50″) we have analyzed the radial dependence of the velocity dispersion. We have repeated the same exercise taking different locations as aperture centers within the image (Figs. 3*a*–3*b*).

For small diameter apertures, between 2″ and 15″, which trace the properties of well-localized parcels of gas one can see different behaviors. The spectra centered in two different positions within the central low-intensity region, cavity A and channel (asterisk and open diamond [◇], in Figs. 3*a*–3*b*), show the highest values of σ within the nebula which decay steeply with increasing aperture (in close agreement with the results of Melnick 1980, his Fig. 1, and Hippelein & Fried 1984, their Fig. 8*b*). On the other hand, when centered in knots 3, 4, and 7 (open triangles, diamonds, and squares, respectively) the value of σ shows a gradual increase with increasing aperture. Knots 1 and 2 (stars and crosses), however, do not present any significant variation as the aperture grows.

All curves of growth for aperture sizes $\geq 30''$ level off to a velocity dispersion value of $\sim$17–18 km s^{-1} in Hα and of $\sim$16–17 km s^{-1} in [O III], in good agreement with earlier Fabry-Perot observations (Smith & Weedman 1970; Melnick 1980; Hippelein & Fried 1984).

4.2. *The Flux-σ Relation*

In order to find the areas that contribute the most to the observed global velocity dispersion value, NGC 604 was divided into 49 square areas of 60.8 arcsec^{-2} each (see Figs. 4*a*–4*b*). To follow a flux conservative procedure, a single spectrum was extracted from each of these areas and were fitted with a single Gaussian profile. Then, all spectra with flux values higher than a certain percentage (40%, then 50%, and finally 70%) of the maximum flux detected on the whole region were independently added and the rest were discarded. No significant differences were found in the velocity dispersion of any of the resulting spectra with respect to that obtained for the whole region. The areas with flux values higher than 70% were then further divided into squares of 15.2 arcsec^2 (Figs 5*a*–5*b*), and the same procedure was repeated with the same grouping criteria. In this way, large sections of the original data set were discarded. Furthermore, even large sectors belonging to the few original 49 larger divisions with a 70% or greater percentage of the maximum flux value were also discarded. The final value of σ derived in this way remained also similar to the global value. Thus the procedure has led to the determination of the zones truly responsible for the global value of the velocity dispersion in NGC 604: the zones that weight the most when producing the global integrated emission-line profile.

The relative contribution to the global value of σ's of all other sectors into which NGC 604 was divided is negligible,

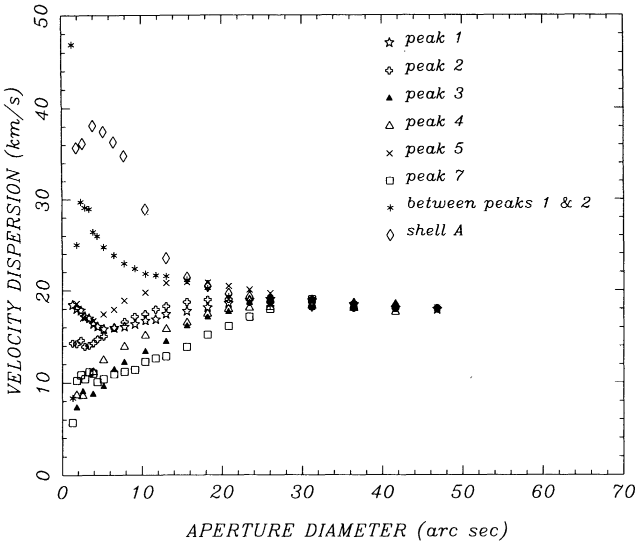

FIG. 3*a*

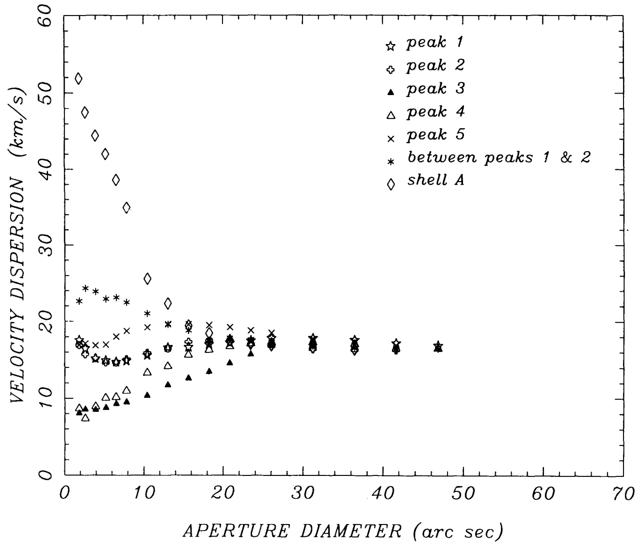

FIG. 3*b*

FIG. 3.—Growth curves of corrected σ vs. aperture diameter for different central positions for (*a*) Hα and (*b*) [O III] λ5007.

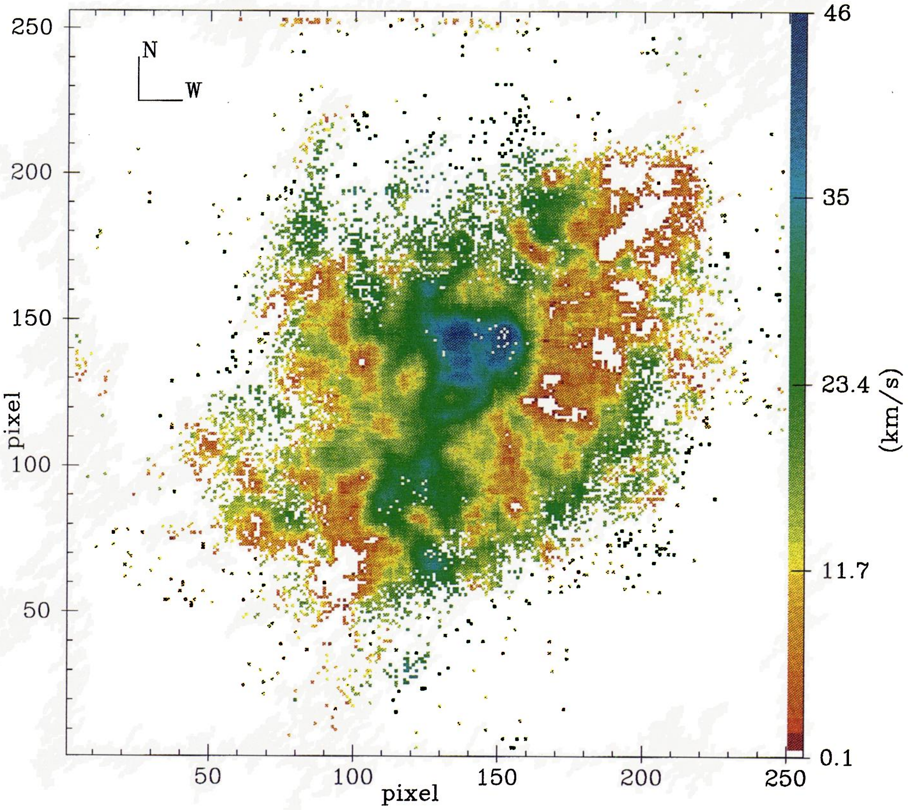

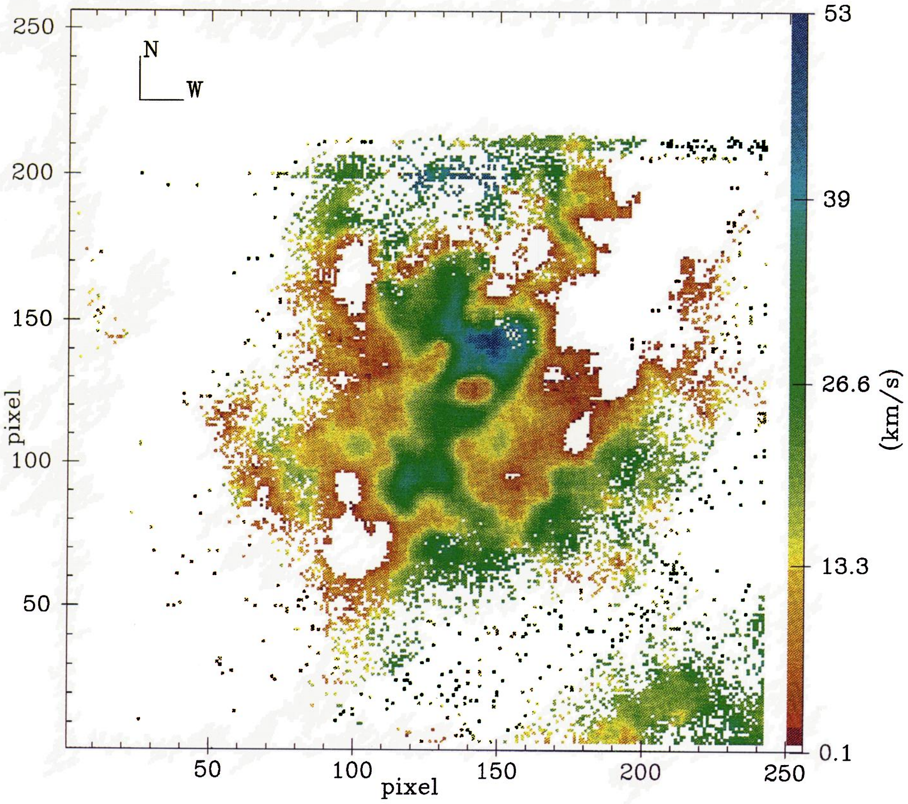

SABALISCK et al. (see 444, 203)

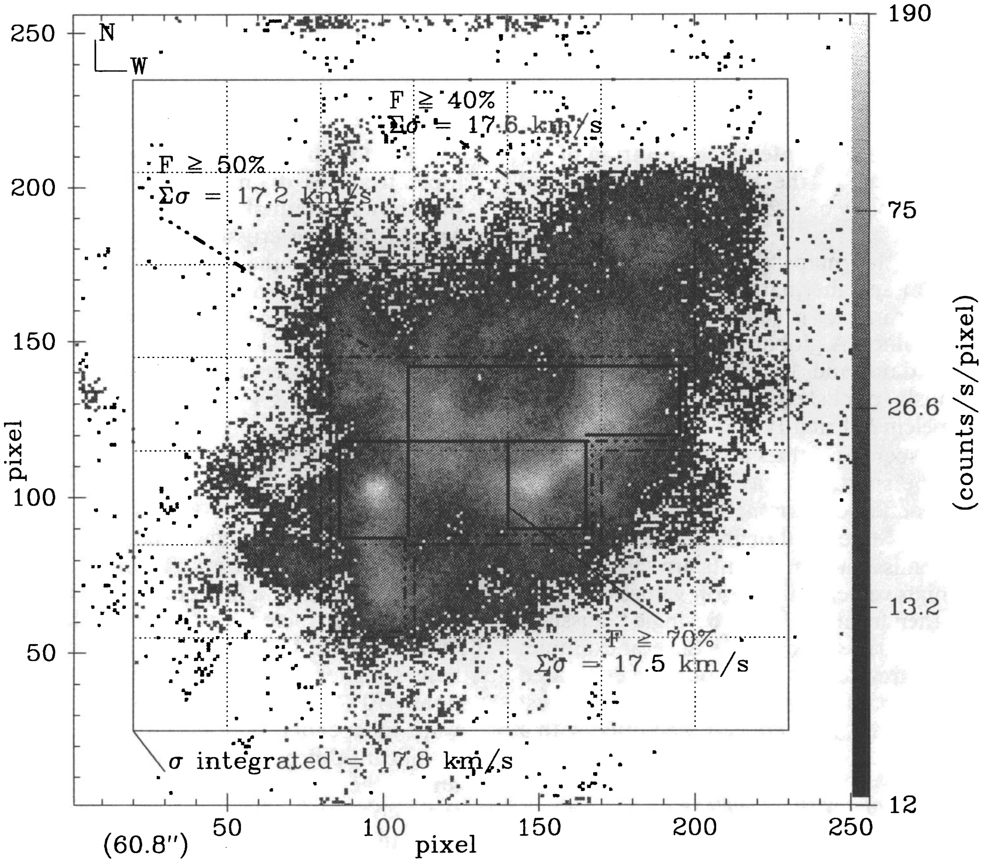

Fig. 4*a*

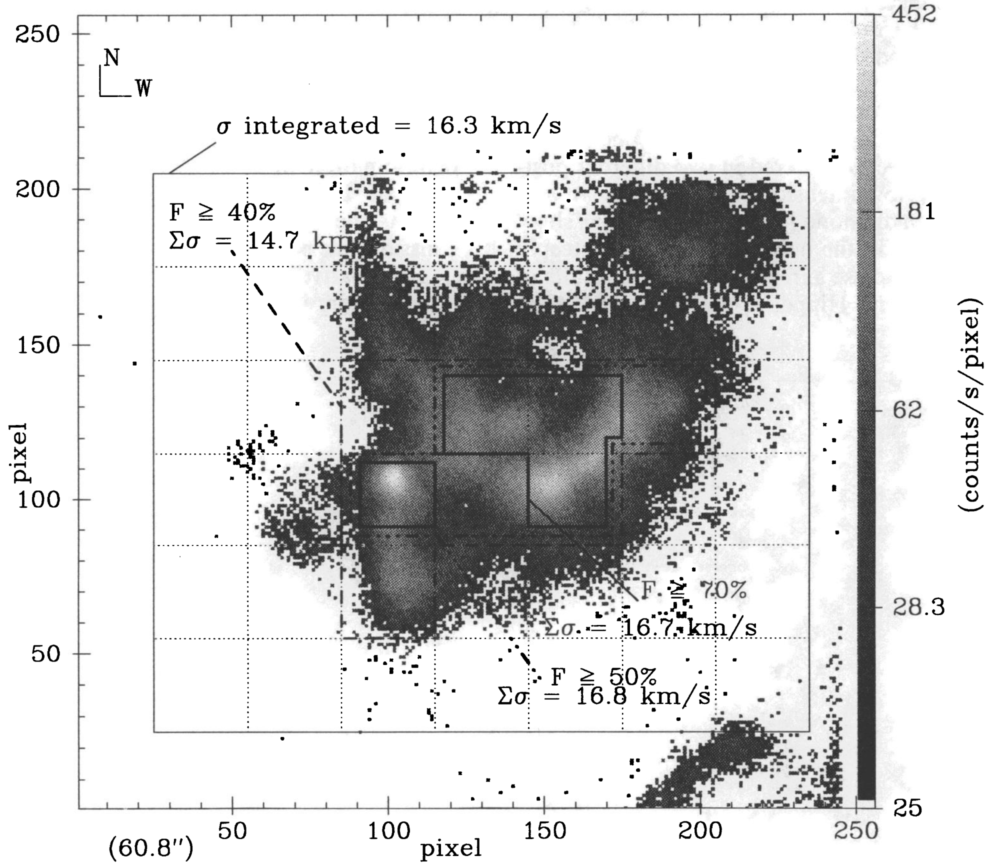

Fig. 4*b*

Fig. 4.—Collapsed image of NGC 604, obtained from the compression of the data cube in the spectral direction, for Hα (*a*) and [O III] (*b*). The 49 square areas of 60.8 arcsec^2 each are indicated with a dotted line. Indicated also are the areas used in the sum with a flux value larger than 40% (*dashed line*), 50% (*dash-dotted line*) and 70% (*solid line*) together with the resultant value of σ. Along the x and y axes 1 pixel = 0″.26 = 0.91 pc.

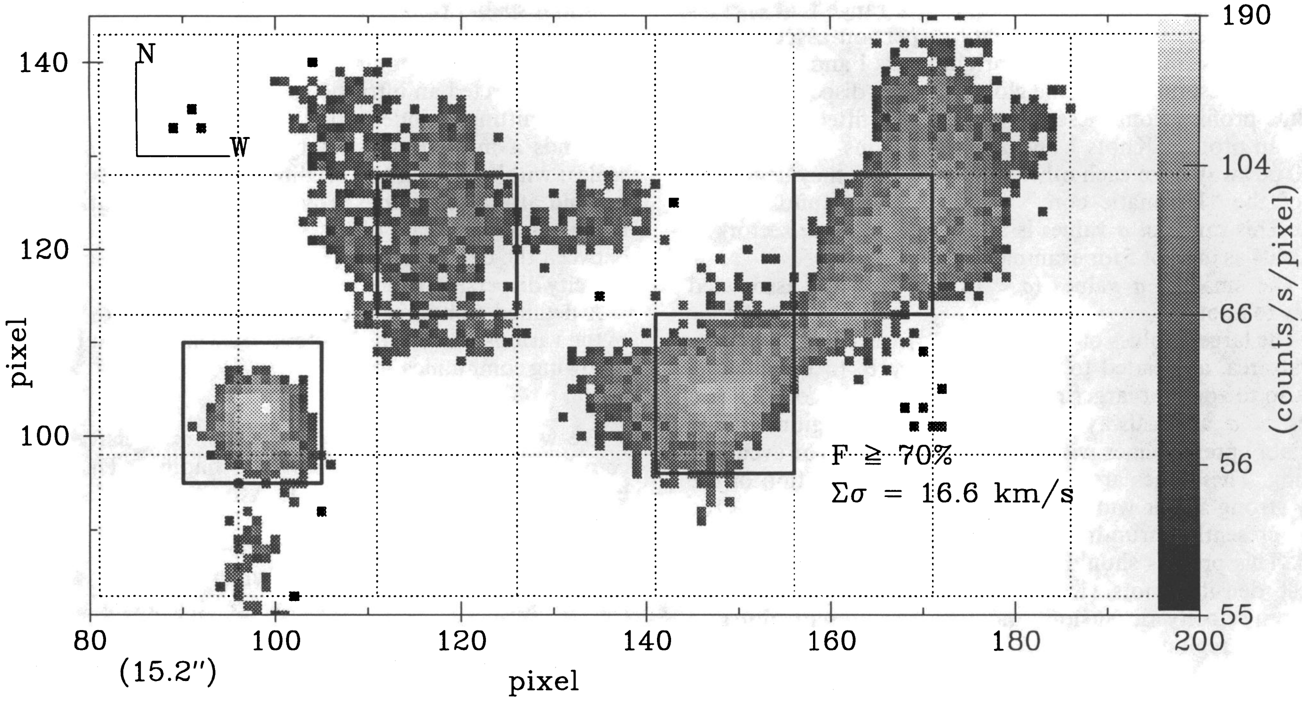

FIG. 5a

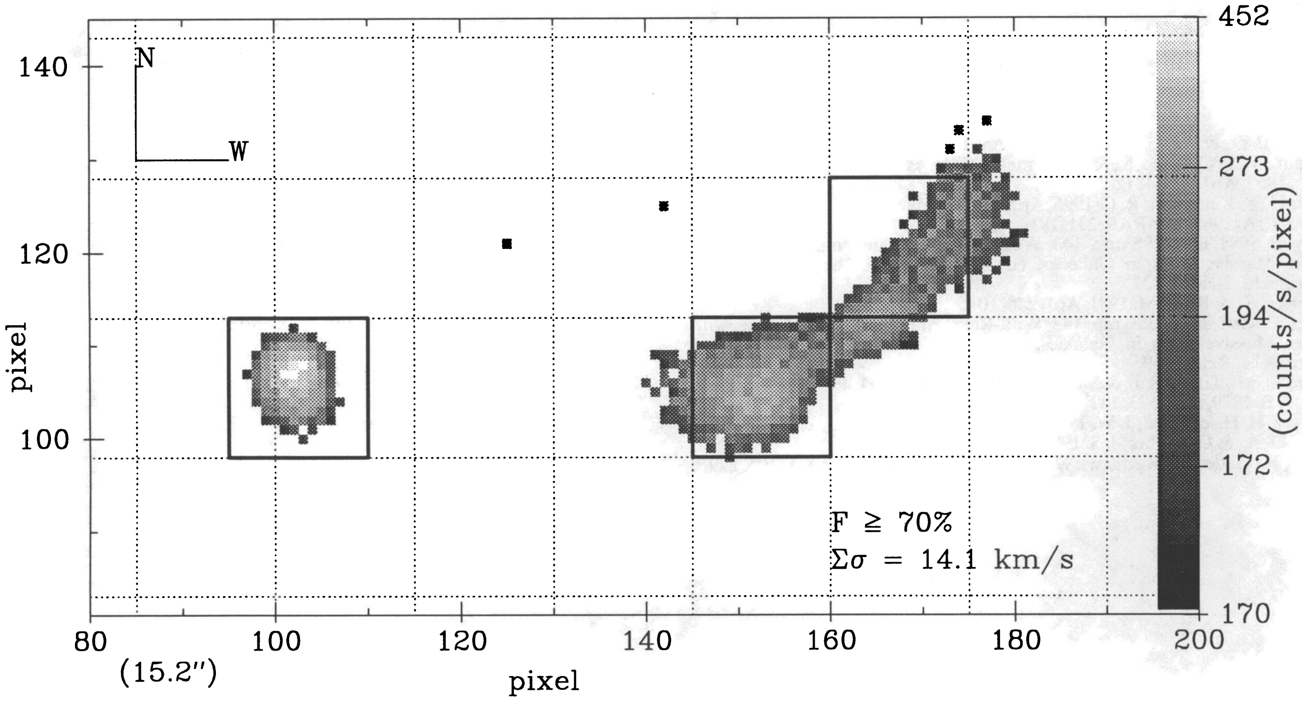

FIG. 5b

FIG. 5.—Collapsed image of NGC 604 for Hα (*a*) and [O III] (*b*), where the most intense areas are plotted. The square areas of 15.2 arcsec^2 are marked with a dotted line. Only the zones with more than 70% of the maximum flux value (marked with a solid line), that contribute significantly to the global value of σ, are shown. Along the x and y axes 1 pixel = 0″.26 = 0.91 pc.

and therefore does not determine the attained value of σ. Many of these sectors present in fact even larger values of σ. However, given their low emission levels, whether they may be located in the central or surrounding areas, their inclusion in the global spectra only changes the value of the global velocity dispersion by less than 10%.

5. CONCLUSIONS

Different values of σ have been found all over NGC 604. However, in a detailed analysis one could differentiate three velocity dispersion ranges, associated with three distinct emitting areas;

1. The values of $14 < \sigma < 20$ km s^{-1}, a range that encompases the supersonic global velocity dispersion associated to NGC 604, arise mainly from the bright knots 1 and 2, and thus are directly responsible for the global velocity dispersion value. The line profiles from these regions are well fitted with single Gaussian profiles. Knots 1 and 2 have a radius of ~ 7 pc and are 50 pc away from each other. Thus, together they define the size of the "kinematic core" of NGC 604 (Muñoz-Tuñón 1994). This range of σ values is also found in other sectors of NGC 604 as in knot 5 for example.

2. The smallest σ values ($\sigma < 14$ km s^{-1}) are associated mainly to knot 3.

3. The largest values of σ (> 20 km s^{-1}) are found within the central area, associated to cavity A, cavity B, to the channel and also to zones at larger radii well outside the "core." These values of σ arise always from low-intensity regions which invariably present lines with strong asymmetries, or even line splitting. These lines are most likely due to the action of the many strong stellar winds caused by the massive stars in the region presently disrupting large sections of the original parent cloud. This process should eventually also come to affect the highest density knots (1 and 2), changing their presently common velocity dispersion, and thus the present global σ value of the region.

The main result of our study is that the global value of σ in NGC 604 arises from the densest (and/or most intense) emitting knots in the center of the region—those that show single Gaussian profiles. This result is not affected by decreasing the bin size of the spectra to the seeing limit (1″). We know from our high spatial resolution data that the radial velocity of the emitting knots is rather similar and thus the global value of σ is not caused by the random motions between the knots. Instead, we have detected an intrinsic velocity dispersion in each of the main emitting condensations. The observation therefore demands a mechanism stirring the gas locally, i.e., in small scales; within each of the brightest emitting knots (radius ≈ 7 pc) and at the same time providing the condensations, within the much larger scale of the "kinematic core" or separation between the densest knots (≈ 50 pc), with the same supersonic velocity dispersion value.

A detailed comparison of the observations with predictions of the various models in the literature will be the subject of our following communication.

We would like to thank the anonymous referee for many comments that helped to clarify our findings. This work has been funded by the Instituto de Astrofisica de Canarias and the Spanish Dirección General de Investigación Científica y Técnica (DGICYT). H. O. C. gratefully acknowledges the DGICYT for a fellowship under which part of this work was carried out. N. S. P. S. acknowledges the financial Brazilian agency CNPq for the doctoral fellowship, and thanks the IAC for hospitality and a grant. G. T. T. and C. M. T. acknowledge partial support from DGICYT (grant PB 91-0531 GEFE) and NATO grant (CRG 92-0198) for collaborative research. The WHT is operated in the island of La Palma by the Royal Greenwich Observatory at the Observatorio del Roque de los Muchachos of the Instituto de Astrofisica de Canarias.

REFERENCES

Atherton, P. D., & Taylor, K. 1980, MNRAS, 191, 675

Benvenuti, P., D'Odorico, S., & Dumontel, 1979, Ap&SS, 66, 39

Blitz, L. 1985, ApJ, 296, 481

Chu, Y.-H., & Kennicutt, R. C. 1995, ApJ, submitted

Clayton, C. A. 1988, MNRAS, 231, 191

Debray, B. 1991, in IAU Symp. 143, Wolf-Rayet Stars and Interrelations with Other Massive Stars in Galaxies, ed. K. van der Hucht & B. Hidayat (Dordrecht: Reidel), 427

D'Odorico, S., & Rosa, M. 1981, ApJ, 248, 1015

Drissen, L. 1991, in IAU Symp. 143, Wolf-Rayet Stars and Interrelations with Other Massive Stars in Galaxies, ed. K. van der Hucht & B. Hidayat (Dordrecht: Reidel), 595

Drissen, L., Moffat, A. F. J., & Shara, M. M. 1990, ApJ, 364, 496

Dyson, J. E. 1979, A&A, 73, 132

Hippelein, H. H., & Fried, J. W. 1984, A&A, 141, 49

Hunter, D. A., & Gallagher, J. S. 1985, AJ, 90, 1457

Israel, P. F., Gatley, I., Matthews, K., & Neugebauer, G. 1982, A&A, 105, 229

Kennicutt, R. C. 1984, ApJ, 287, 116

Lewis, J., & Unger, S. W. 1992, in ASP Conf. Ser., Vol. 25, Astronomical Data Analysis Software and Systems. I., ed. D. M. Worral, C. Biemesderfer & J. Barnes (San Francisco: ASP), 445

Melnick, J. 1980, A&A, 86, 304

Melnick, J. 1992 in Proc. 3d Canary Island Winter School of Astrophysics, Star Formation in Stellar Systems, ed. G. Tenorio-Tagle, M. Prieto, & F. Sánches (Cambridge: Cambridge Univ. Press), 255

Muñoz-Tuñon, C. 1994, in Violent Star Formation from 30 Doradus to QSOs, ed. G. Tenorio-Tagle (Cambridge: Cambridge Univ. Press), 25

Rosa, M., & Solf, J. 1984, A&A, 130, 29

Skillman, E., & Balick, B. 1984, ApJ, 280, 580

Smith, M., & Weedman, D. 1970, ApJ, 161, 33

Tenorio-Tagle, G., Muñoz-Tuñón, C., & Cox, D. P. 1993, ApJ, 418, 767

Terlevich, R., & Melnick, J. 1981, MNRAS, 195, 839

Wright, M. C. H. 1971, ApJ, 7, L209